

# Specific versus non-specific solvent interactions of a biomolecule in water

Lanhai He,<sup>1,2</sup> Sebastian Malerz,<sup>3</sup> Florian Trinter,<sup>3,4</sup> Sebastian Trippel,<sup>1,5</sup> Lukáš Tomaník,<sup>6</sup>  
Michal Belina,<sup>6</sup> Petr Slavíček,<sup>6,||</sup> Bernd Winter,<sup>3,§</sup> and Jochen Küpper<sup>1,5,7,\*</sup>

<sup>1</sup>Center for Free-Electron Laser Science, Deutsches Elektronen-Synchrotron DESY, Notkestraße 85, 22607 Hamburg, Germany

<sup>2</sup>Institute of Atomic and Molecular Physics, Jilin University, 130012 Changchun, China

<sup>3</sup>Fritz-Haber-Institut der Max-Planck-Gesellschaft, Molekülphysik, Faradayweg 4-6, 14195 Berlin, Germany

<sup>4</sup>Institut für Kernphysik, Goethe-Universität Frankfurt, Max-von-Laue-Straße 1, 60438 Frankfurt am Main, Germany

<sup>5</sup>Center for Ultrafast Imaging, Universität Hamburg, Luruper Chaussee 149, 22761 Hamburg, Germany

<sup>6</sup>Department of Physical Chemistry, University of Chemistry and Technology, Technická 5, 16628 Prague, Czech Republic

<sup>7</sup>Department of Physics, Universität Hamburg, Luruper Chaussee 149, 22761 Hamburg, Germany

Solvent interactions and specifically hydration are of utmost importance in chemical and biochemical systems. Model systems enable us to unravel the microscopic details of these interactions. Here, we clearly unraveled a specific hydrogen-bonding motif of the prototypical biomolecular building block indole ( $C_8H_7N$ ), the chromophore of tryptophan, in water: The system exhibits a strong localized N-H $\cdots$ OH<sub>2</sub> hydrogen bond, but otherwise unstructured interactions of the molecule with the solvent. This surprising segmentation of the solvent interaction was obtained from a combined experimental and theoretical investigation of the electronic structure of indole in aqueous solution. We recorded the complete x-ray photoemission and Auger spectrum of aqueous-phase indole and quantitatively explained all peaks with the aid of extensive *ab initio* modeling. The combination of the maximum-overlap method with the non-equilibrium polarizable-continuum model was demonstrated as an efficient and accurate technique for a modeling of both the valence and core photoemission spectra. A two-hole electron-population analysis shows a quantitative theoretical description of Auger spectra. Especially the core-electron binding energies for nitrogen and carbon demonstrated the distinct specific interaction of the one hydrogen-bound water molecule with the N-H group and the otherwise unspecific solvent interactions. The valence photoemission data provided the reorganization energy of aqueous-phase indole associated with its ionization, which we could directly connect to its electrochemical redox potential.

## INTRODUCTION

Indole ( $C_8H_7N$ ) is an ubiquitous component of peptides and proteins as it is the sidechain chromophore of the essential amino acid tryptophan. Indole has various signaling functions [1–3], but more significantly in the present context, it is an important chromophore of proteins [4, 5]. It starts to absorb strongly below 300 nm, with the main bands around 287 and 217 nm, both corresponding to  $\pi^* \leftarrow \pi$  transitions. The influence of solvation on indole’s electronic structure has long been debated [6], in particular with respect to its two lowest-energy  $^1L_a$  and  $^1L_b$  electronically excited singlet states [7–9]. Microsolvation experiments with one or a few water molecules attached have shed some light onto this topic [10–13].

A natural role of tryptophan is the radiation protection of nucleic acids, e. g., as a near-UV-absorbing building block of the eumelanin polymer [14, 15]. Indole became one of the widely studied model systems to understand the photochemistry of heteroaromatic systems, in particular, the role of the  $\pi\sigma^*$  states [1]. The excited states and photodynamics of gaseous indole were studied by a large variety of techniques, including high-resolution spectroscopy [8, 9, 16], pump-probe laser spectroscopy [17, 18], ion imaging [19], and *ab initio* calculations [20]. Radiation below 300 nm has the potential to cause pyrimidine dimerization, e. g., leading to melanoma [21]. Most damaging is radiation around 250 nm, corresponding to a

minimum of the indole absorption spectrum.

Much less is known on the role of indole in radiation protection in the context of ionizing radiation. While the nucleic acids in solution dominantly suffer radiation damage indirectly, via reactions with OH radicals and hydrated or pre-hydrated electrons formed upon irradiation of water [22, 23], they can be also ionized directly [24, 25]. Then, charge migration and transfer takes place and indole can be one of the sinks for the positive holes formed [26, 27]. Detailed knowledge of the electronic structure and electrochemical quantities is needed to understand these processes and related redox potentials and reorganization energies. Redox properties of indole were studied for decades using kinetic techniques. For example, kinetics measurements enabled to assign the reduction potential of the indole cation to 1.24 V [28]. The ionization onset of indole was determined to 4.35 eV [29].

There were multiple experimental and theoretical studies of indole’s photoelectron spectrum in the gas phase [30–34]. Recently, the electronic structure of indole was investigated in a combined experimental and theoretical study [34], using tunable x-ray radiation and *ab initio* electron propagation and density functional theory. The HOMO and HOMO–1 binding energies were estimated to be 7.90 and 8.32 eV, both corresponding to the ionization through the  $\pi$  orbitals. The electrons in  $\sigma$  orbitals started to be ionized above 11 eV. Core-electron binding energies were characterized as well [34].

The complete electronic structure of indole in the solvent environment, and particularly in water, has not been reported so far. The resonant two-photon ionization (R2PI) spectrum of aqueous indole, exploiting indole’s strong near-UV absorption, was measured and yielded a value of 7.4 eV for the first ionization energy [35], which corresponds to a solvent shift of  $\sim 0.5$  eV. No comparable energy shift was observed for the second ionization energy.

Here, we used an x-ray synchrotron source combined with a liquid microjet to record the full photoemission spectrum, including valence, core, and Auger electrons, of indole in aqueous solution. The x-ray/liquid-microjet combination proved useful in providing accurate insight into the electronic structure of various molecular species, including nucleic acids, organic chromophores, anions, cations, and transition metal complexes [36–38]. The valence part of the spectrum will be interpreted in the context of the electrochemical data discussed above, which provides an independent estimate of the redox properties of indole. The core-level and Auger energies are element-specific and are sensitive to the specific chemical environment. We demonstrate that this concept can be extended even to the domain of non-covalent interactions: We disentangled the non-specific effects, brought about by the long-range solvent polarization, and the specific effects, related to the granularity of the solvent environment, e.g., hydrogen bonding with the nearest solvent molecules. The detailed inspection of the whole photoemission spectrum provided an additional view on the character of solvation interaction for different parts of the indole molecule.

The experimental data were interpreted with an extended *ab initio* modeling of hydrated indole. It was demonstrated previously that present-day computational techniques provide a reliable estimate of the energetics for both the valence and core electrons in the liquid phase, even with simple dielectric-continuum models [39–41]. Special care must be paid to a proper treatment of the non-equilibrium character of the ionization process. In the present work, we demonstrated the wide applicability of the so-called maximum-overlap method [42], enabling us to model the ionized states with the standard ground-state quantum-chemical methods.

## EXPERIMENTAL SETUP

The x-ray photoelectron spectroscopy experiments were carried out at the P04 beamline of the PETRA III synchrotron-radiation facility at DESY [43]. Experimental details of the liquid microjet and photoelectron spectrometer as part of the “Electronic structure of Aqueous Solutions and Interfaces” (EASI) setup were described elsewhere [44]. Briefly, solutions were prepared by mixing highly demineralized water ( $18.2 \text{ M}\Omega \cdot \text{cm}^{-1}$ ) and

17 mM indole (Sigma-Aldrich,  $>99\%$ , used without further purification). Sodium chloride (50 mM) was added to minimize the streaming potential caused by electrokinetic charging [45–51].

A liquid jet of  $\sim 28 \mu\text{m}$  diameter, with a velocity of  $\sim 60 \text{ m/s}$  from a fused-silica nozzle, is generated using a high-performance liquid chromatography (HPLC) solvent delivery pump with a constant flow rate and backing pressure. The beam was captured/dumped in vacuum using a cryopump. The indole-water solution temperature was estimated to be in the range of 279–283 K in the laminar part, which typically exists for  $\sim 10 \text{ mm}$  after the jet injection from the capillary into vacuum [45].

The synchrotron light beam, with a photon energy of 600 eV and a focal size of  $180 \mu\text{m}$  in the horizontal direction (parallel to the liquid jet) and  $35 \mu\text{m}$  in the vertical direction (perpendicular to the liquid jet), intersected the jet perpendicular to the flow of the solution. The small focal size allowed for matching the spatial overlap with the liquid jet and thereby keeping the signal contributions from ionization of gas-phase water molecules surrounding the jet low. The excitation was carried out with circularly polarized light, and a backward-scattering electron-detection geometry, corresponding to an angle of  $130^\circ$  with respect to the light propagation direction, i.e., near magic angle, as detailed elsewhere [44]. The emitted photoelectrons passed from the main interaction chamber, operated at  $10^{-4}$  mbar, through a  $800 \mu\text{m}$  diameter orifice to the differentially pumped detector chamber, operated at  $\sim 10^{-8}$  mbar, which housed a hemispherical electron energy analyzer equipped with a microchannel-plate detector. The small jet diameter in conjunction with the small distance of  $800 \mu\text{m}$  between the liquid jet and the orifice assured that a significant fraction of detected electrons did not inelastically scatter with water gas-phase molecules near the jet surface [45, 46]. The energy resolution of the P04 beamline was better than 250 meV. The energy resolution of the hemispherical analyzer was better than 200 meV. Therefore, the total energy resolution was better than 320 meV. Tuning the detecting kinetic-energy range of the hemispherical electron energy analyzer, we experimentally obtained the photoelectron spectra (PE spectra) from aqueous indole’s valence band (VB) as well as from core ionization of the nitrogen and carbon  $1s$  orbitals, including the Auger electrons.

## THEORETICAL METHODS

Photoelectron spectra were modeled within the nuclear-ensemble method, which can be viewed as a particular realization of the reflection principle, i.e., by projecting the nuclear density in the electronic ground state onto the ionized state and further onto the spectrum of ionization energies [52–54]. The ground-state density of indole was estimated within the path-integral molecular-

dynamics method, accelerated with the quantum thermostat based on the generalized Langevin equation [55] (PI+GLE method). In this way, the delocalization due to the nuclear-quantum effects was taken into account. The simulation was done at the BLYP/6-31G\* level of the electronic-structure theory, representing an efficient combination for large number of calculations during the MD simulation. A time step of 0.5 fs was used and four replicas were propagated. The total duration of the simulation was 23 ps, with the first 5 ps used for equilibration. In total, 100 indole geometries were used for subsequent calculations. PI+GLE simulations were performed using our in-house code ABIN [56] connected to the Terachem software (version 1.93) [57, 58].

Core-level ionization spectra were calculated at the MP2 level of theory with the cc-pCVTZ basis set (designed specifically for core states) for carbon and nitrogen atoms and a corresponding cc-pVTZ basis set for hydrogen atoms. For modeling the core-ionized states, we have used the maximum-overlap method (MOM) [42] as implemented in the Q-Chem software (version 4.3) [59]. The aqueous solution was mimicked by the non-equilibrium polarizable-continuum model with integral equation formalism (IEF-PCM) [60] with the atomic radii from universal force field (UFF) [61]. In total, core-ionization energies from 100 sampled geometries were obtained for every atom, i. e., one nitrogen and eight carbon atoms. The PE spectra of aqueous-phase indole were constructed as a sum of Gaussian functions centered at the respective calculated value of the ionization energies for each geometry. The standard-deviation parameter for every single Gaussian was set to 0.32 eV, obtained using the additional broadening model [62], and corresponds to the additional broadening arising from different configurations of solvating water molecules that were not explicitly included in our calculations. The model required the reorganization energy of water molecules solvating indole, which we calculated as a difference between the energies calculated with the equilibrium and non-equilibrium versions of the PCM solvation model for the optimized indole geometry. The gas-phase PE spectra were generated with the same procedure except for the standard-deviation parameter that was set according to the Silverman’s rule of thumb [53, 63].

The valence-ionization spectrum was calculated using the long-range-corrected Perdew–Burke–Ernzerhof functional (LC- $\omega$ PBE) [64] with the aug-cc-pVDZ basis set. The range-separation parameter  $\omega$  was optimized to the value of  $0.3 a_0^{-1}$  on the set of 100 indole geometries using the ionization-potential theorem, i. e., minimizing the difference between ionization energies obtained as the energy of the HOMO and as the difference between electronic energies of ground and ionized state [65, 66]. Using the optimized parameter  $\omega$ , the first two ionization energies were subsequently calculated for each geometry with the MOM approach. The photoelectron spectrum was generated by

the same procedure described above.

Furthermore, we explored the influence of involving explicit water molecules into our calculations on the resulting ionization energies. To do so, we (i) calculated ionization energies of solvated clusters containing the indole molecule with one to three explicit water molecules, (ii) we executed the molecular-dynamics simulation of indole involving explicit water molecules and then calculated the valence-ionization spectrum for snapshots of the MD simulation. Ad (i), the microhydrated clusters were optimized at the MP2/cc-pVTZ level of theory, and core- and valence-ionization energies for the minimal geometries were calculated using the same approach as described above. Ad (ii), the molecular-dynamics simulation was performed for a droplet of indole in water, using the QM/MM approach with the quantum part containing the indole molecule and the MM part consisting of 500 water molecules. The QM part was described at the BLYP/6-31g\* level with Grimme’s dispersion correction D2 [67], the MM part was described with the TIP3P water model [68, 69]. Calculations were performed at the standard temperature of 298.15 K during the whole simulation by the Nosé–Hoover thermostat. The QM/MM simulation was performed using our code ABIN connected to the Terachem software (version 1.93), the initial arrangement of water molecules was obtained using the Packmol code [70]. The total duration of simulation was 25 ps with time steps of 0.5 fs. From the last 20 ps, 100 geometries were sampled with equidistant steps, i. e., every 200 fs. We have then extracted the coordinates of the indole molecule without water molecules and with its closest 20 water molecules, respectively. Those structures were then used to calculate the valence-ionization spectrum following the procedure described above (including PCM) to inspect the influence of explicit water molecules on calculated valence-ionization energies.

The Auger spectra were calculated in the following way. We first evaluated the onsets of the spectra within the MOM method with correlated wavefunctions and then we modeled the higher transitions with a simpler *ab initio* approach based on the complete active space configuration interaction (CAS-CI) wavefunction expansion. The onset of the Auger spectrum was calculated as a difference between the core-ionized and double-valence-ionized electronic energies calculated at the MP2 level with the cc-pCVTZ basis set for N and C atoms and the cc-pVTZ basis set for H atoms. The calculations of the energies for modeling the Auger spectrum were only performed on a single geometry optimized at the MP2/cc-pVTZ level using the Q-Chem software (version 4.3) [59]. The Auger intensities were estimated within the qualitative approximate scheme based on the Mulliken population analysis [71]. In this method, relative transition rates are approximated using atomic populations of valence orbitals of particular final states on core-ionized atoms. The valence orbitals are constructed by the CAS-CI method and

the cc-pVTZ-f basis on the neutral-ground-state wavefunction. The kinetic energies of the Auger electrons  $E_i$  were evaluated as

$$E_i = E_{1s} - E_{2h,i} \quad (1)$$

where  $E_{1s}$  is the energy of the core-ionized state and  $E_{2h,i}$  is the energy of the final two-hole state. Note that we start with core-ionized states localized on different atoms, eight carbons and one nitrogen in total. The line spectra consisting of energies and intensities from the contribution of every final state were broadened with a Gaussian distribution with a standard-deviation width of 2 eV to reproduce the broadening observed in the experiment. The calculations were performed in the TeraChem software (version 1.93) [57, 58].

## RESULTS AND DISCUSSION

### Valence photoemission

The PE spectrum of the valence band (VB) of an indole-water solution, measured at a photon energy of

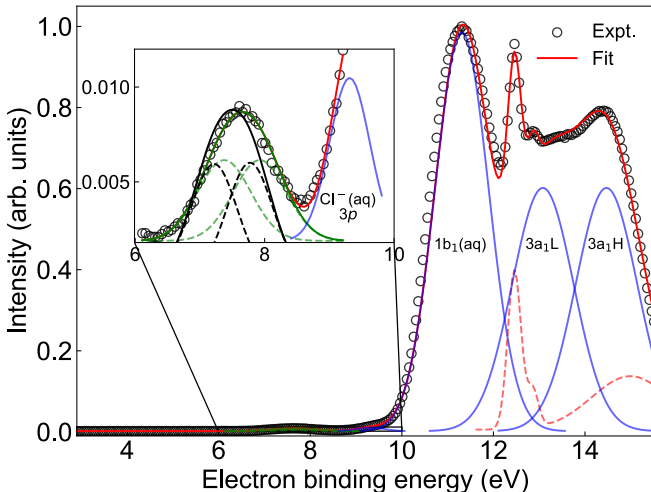


FIG. 1. Experimental valence-photoemission spectrum of aqueous indole (gray empty circles). The solid red line represents the overall fit. The contributions from the  $1b_1$  and  $3a_1$  molecular orbitals of liquid water, with the  $3a_1$  components  $3a_{1L}$  and  $3a_{1H}$ , and  $\text{Cl}^- (3p)$  of sodium chloride background are indicated in the figure with blue solid lines. A broken red line indicates the contributions from gaseous  $\text{H}_2\text{O}$ . The inset shows the details in the binding-energy region between 6 and 10 eV with the indole photoemission signal. The experimental data were either fitted with one Gaussian (green solid line) or with two Gaussians (green dashed lines) representing the signal from HOMO and HOMO-1 orbitals of aqueous indole, see text for details. The black solid line represents the calculated valence spectrum of aqueous indole, and the black dashed lines represent the calculated components from HOMO and HOMO-1.

TABLE I. Vertical ionization energies (VIE) of aqueous and gaseous indole, in units of eV.

	Exp. <sup>aq</sup>	Calc. <sup>aq</sup>	Exp. <sup>g</sup> <sup>a</sup>	Calc. <sup>g</sup>
HOMO	7.38	7.22	7.90	7.86
HOMO-1	7.93	7.77	8.35	8.34

<sup>a</sup> VIE reported for indole in the gas phase [34].

600 eV, is shown in Fig. 1. The raw spectrum was energy-calibrated [72] and intensity-normalized against the liquid water  $1b_1$  peak at 11.33 eV [51, 73–78]. Photoemission signals (gray empty circles) are fitted with multiple Gaussian functions, representing the contributions from the involved atomic and molecular orbitals, and the red solid line represents the overall fit.

By comparing the valence-band PE spectrum of the indole-water solution to that of a 50 mM NaCl solution in water, we identified the emerging peak that exclusively corresponds to aqueous indole, shown in the inset of Fig. 1 with fitted contributions (green lines). We used two approaches for fitting the measurement, i. e., either one Gaussian or two Gaussians. The binding energy extracted from the single-Gaussian fit is 7.65(1) eV with a full width at half maximum (FWHM) of 1.18 eV. The spectral width reflects, in a non-trivial way, the reorganization energy of the solute upon single ionization. However, the observed 1.18 eV value is significantly larger than to be expected for aromatic molecules of similar size in solution [37]. Therefore, this immediately indicates that this band corresponds to the ionization from multiple orbitals, i. e., the peak spans at least two close-lying molecular orbitals. This tentative conclusion is supported by the corresponding gas-phase data, showing the HOMO and HOMO-1 orbitals to be separated by merely 0.45 eV, see Tab. I; the conclusion is further supported by the *ab initio* calculations as we discuss below. The energies of these two orbitals (green dashed lines in the inset of Fig. 1) have been extracted, from a fit using two Gaussians, to be 7.38 and 7.93 eV with a FWHM of 0.97 eV; the difference between the HOMO and HOMO-1 energies was fixed to 0.55 eV based on our calculations, see details below, and the amplitudes of the two transitions were set to be identical, assuming the same cross sections for ionization from HOMO and HOMO-1 orbitals of indole.

Upon transfer of the molecule from the gas phase into aqueous solution, the ionization energy is expected to be shifted due to the polarizable environment [79]. The extent of the solvent shift is controlled by the relative stabilisation of the initial neutral ground state and the final radical-cation state in water. A typical shift observed for aromatic molecules of a size similar to indole is on the order of 1 eV [37].

Our calculated valence-ionization energy in the gas phase agrees excellently with the experimental data of Plekan *et al.* [34] with a discrepancy in binding en-

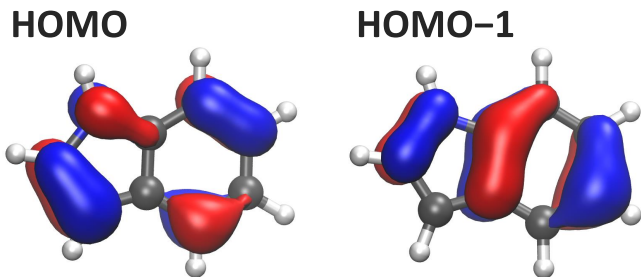


FIG. 2. Calculated highest occupied molecular orbital (HOMO) and second-highest occupied molecular orbital (HOMO-1) of aqueous indole. Both orbitals are of  $\pi$  character and are delocalized over the molecule.

ergies of less than 0.05 eV, see Tab. I. The calculated aqueous-phase valence spectrum including HOMO and HOMO-1 contributions, Fig. 1 (black solid line in the inset), has its maximum at 7.50 eV, differing from the experimental aqueous-phase data by 0.15 eV. This is a very good agreement; the remaining discrepancy is to be attributed to the treatment of solvation. The observed shift in the present case is on average  $\sim 0.47$  eV for HOMO and HOMO-1 orbitals, see Tab. I. The exact value slightly depends on the fitting procedure. However, it is surprisingly small, suggesting competing specific and non-specific solvent effects. The calculated spectrum exhibits the spectral shape which is in good agreement with the present experiment. Note that the calculated spectra were generated within the cluster-continuum model, i. e., the solvent was described as a polarizable continuum while, simultaneously, the 20 nearest water molecules were included in the calculations. If these explicit molecules were excluded, the maximum of the calculated photoelectron peak would be shifted to 7.38 eV, compared to 7.50 eV. This identified certain specific solvent effects, manifested by a difference of 0.12 eV, even though the majority of the shift is due to solvent polarization. These specific solvent effects are responsible for the relatively small solvent shift observed in the experiment compared to similar molecules.

The calculations reveal that the aqueous-phase valence band actually consists of two transitions corresponding to two different orbitals, both of them of  $\pi$  character, see Fig. 2. The difference in the peak positions based on our calculations is estimated to be 0.55 eV. This is somewhat larger than the 0.45 eV splitting for the gas-phase experiment, which is reproduced very well by our *ab initio* calculations. However, the discrepancy is not significant when we consider the inaccuracies in the calculations and the errors introduced by the fitting procedure for the experimental data.

Let us now focus on the interplay between specific and non-specific solvent interactions. An interesting insight is brought about by the inspection of the indole-water dimer complex in the gas phase. The global minimum of this complex corresponds to the hydrogen-bonded struc-

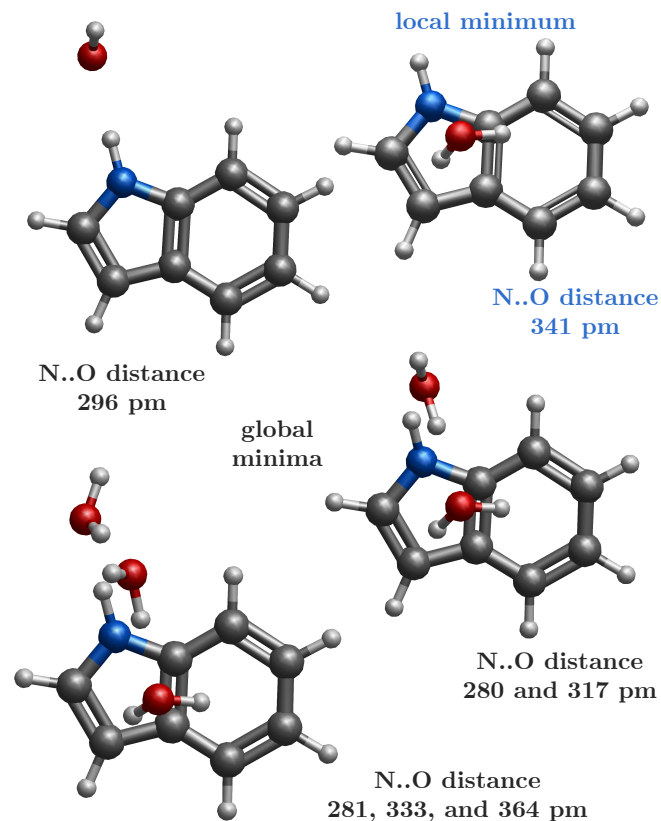


FIG. 3. Optimized structures of gas-phase indole-water clusters containing one, two, and three water molecules. At least one water molecule forms hydrogen bond with the N-H group while others are pointing towards the  $\pi$  ring.

ture via the N-H  $\cdot$  O contact [10], see also Fig. 3. This complex has a calculated vertical ionization energy (VIE) of 7.51 eV and an adiabatic ionization energy (AIE) of 7.27 eV. These calculations can be compared with the available experimental data, where R2PI experiments provided AIEs of the bare indole molecule as well as the cluster of indole with one water molecule of 7.76 and 7.34 eV, respectively [80]. The energetic drop of about 0.4 eV in experimental AIE when adding the first water molecule is also observed in our calculations of VIEs, which drop from 7.87 to 7.51 eV, see Tab. III. Water molecules can, however, also bind to the  $\pi$  system of the indole molecule, see Fig. 3. The hydrogen-bonded complex is energetically preferred by 0.1 eV according to our calculations. VIE for this complex is calculated to be 0.6 eV larger while the adiabatic energy is only 0.3 eV larger than for the  $\pi$ -system-bound structure. Thus, the reorganization energy is larger for the dimer with the water molecule bound to the  $\pi$  system of indole than for the hydrogen-bonded system. At the same time, the optimized structure of the oxidized indole-water complex is very different from the neutral structure in this case.

In liquid water, the water molecules are positioned

around the whole indole molecule. One of the water units is certainly located in the hydrogen-bonded position as it is documented by the core-level ionization spectrum, see section “Core-electron binding energies“ below. Most other water molecules are, however, placed above or below the  $\pi$  ring of the indole system. In those positions, the water molecules will need to dramatically reorganize upon the ionization, which will lead to a pronounced reorganization energy and decreasing value of the Franck–Condon overlap for the states energetically close to AIE. The water molecules surrounding the  $\pi$  system also contribute to the increase of VIE, counterbalancing the VIE decrease by long-range polarization. As a result, the solvent shift is smaller than expected from the dielectric theory or from our experience with organic molecules of a similar size.

Additionally, we compared our results with previously reported experimental data for aqueous-phase indole, also in a liquid jet, obtained from single-color resonance-enhanced two-photon ionization (R2PI) [35]. In that experiment, two different wavelengths, 266 and 292 nm, were used and the obtained spectra were fitted by one or two Gaussians to extract the first and second vertical ionization energies (VIE) as 7.4 eV and 8.4 eV, respectively. Note that both values were obtained by applying a correction for inelastic scattering to the measured peaks. The first ionization energy is in very good agreement with our data, i. e., consistent with the solvent shift of 0.5 eV (*vide supra*). However, the value of the second ionization energy [35] would almost coincide with the respective gas-phase energy, see Tab. I. This would indicate the absence of a solvent shift, which does not seem likely. Indeed, our measured value of 7.93 eV corresponds to a solvent shift of 0.41 eV, consistent with the value for the first ionization energy. The discrepancy between the x-ray and the R2PI measurements can be attributed to spectral distortions in the latter case due to large cross sections for quasi-elastic scattering between the emitted slow photoelectrons and water molecules in the solution [81]. A retrieval of the exact native, undistorted peak position [35] from UV-ionization measurements appears to be rather challenging. There could be additional contributions resulting from pulse-duration dependencies introduced by the electronic relaxation during the laser pulse.

### Electrochemical redox potential

The measured valence-photoemission data can be compared to results from electrochemical and kinetic experiments. Our data provide VIE, which reflect the vertical photoionization process when the electron is ejected without changing the molecular geometry either of the solute or solvent: It is a non-equilibrium quantity. Redox potentials are related to the energetics of the ionization as well, yet it is the equilibrium free-energy change controlling the value of the redox potential. The absolute redox potential

$E$  can be converted into the AIE as

$$\text{AIE} = -zFE \quad (2)$$

where  $z$  is the number of exchanged electrons and  $F$  is the Faraday constant,  $E$  is the redox potential of the respective oxidation process, e. g.,  $\text{C}_8\text{H}_7\text{N} \rightarrow \text{C}_8\text{H}_7\text{N}^+ + e^-$ .

The difference between the VIE and AIE is the reorganization energy  $\lambda$  and corresponds to the free energy released by the rearrangement of molecular geometries of solute and solvent following the non-equilibrium ionization, e. g., photoionization. The reorganization energy can be relatively easily obtained for isolated gas-phase molecules. For indole, zero-electron-kinetic-energy (ZEKE) spectroscopy [82], R2PI [80], and XPS [30] data reported the AIE of gas-phase indole to be 7.76, 7.76, and 7.75 eV, respectively. When combined with the computed VIE of 7.86 eV, we get a gas-phase reorganization energy of 0.1 eV. Our *ab initio* calculations confirm this value of  $\sim 0.15$  eV. The reorganization energy is much larger in the liquid phase. The value of reorganization energy could be the route to connect liquid-phase photoemission spectroscopy and electrochemistry. Unfortunately, the determination of the onset of the PE spectra, and thus of AIE, is not easy and rather ambiguous. We can only coarsely estimate the onset to be  $\sim 6.4$  eV. The value is consistent with the onset of the R2PI spectra [35], estimated to be either 6.2 eV (266 nm) or 6.0 eV (292 nm). Thus, the reorganization energy is estimated to be 1.0 eV.

We can now compare the adiabatic ionization energy with the data from kinetic measurements. Here, the one-electron reduction potential of the indole cation was found to be 1.24 V [28] *versus* a standard hydrogen electrode (SHE). This value is not far from our calculated value of 1.32 V using the COSMO-RS approach, which typically provides accurate values of the redox potentials [83, 84]. Considering the absolute reduction potential of SHE to be 4.28 V [85], we obtain the absolute reduction potential of the indole cation of 5.52 V. This corresponds to the absolute *oxidation* potential of neutral indole of  $-5.52$  V since oxidation and reduction are reverse processes. Using (2), we obtain an AIE of 5.52 eV, which is lower than the threshold values measured via either XPS or R2PI. However, the experimental assignment of the redox potential is difficult due to a possible subsequent proton-transfer reaction. On the other hand, the  $pK_a$  value of the oxidized indole radical was suggested to be 4.9 [28] and there should be no proton transfer immediately following the oxidation of indole. Observations of the formation of indole trimers following the electrooxidation of indole [86] bring a further uncertainty into the experimental data.

Electrochemical data also provide the edge ionization potential of indole, which again corresponds to the AIE, with a value of 4.35 eV [29]. However, in that experimental setup a solvated electron has been produced and the solvation energy of the electron is rather uncertain [87].

Proposed values vary from -1.92 to -1.42 eV, leading to values of AIE from 5.77 to 6.27 eV.

Nevertheless, it seems more likely that there is a true and significant difference between the AIE and the threshold of the PE spectrum. We assign this to very small Franck-Condon factors at the onset of ionization. As the photoemission in the gas phase is dominated by  $0 \rightarrow 0$  transition we ascribe this to a strong contribution of the solvation environment.

### Core-level binding energies

The core-level PE spectra of aqueous indole from the carbon and nitrogen  $1s$  edges are shown in Fig. 4 together with a fit of a sum of multiple Gaussians to this data. The raw spectra were background-corrected by subtracting second-order polynomials to describe the contributions of the scattered electrons.

The  $C(1s)$  PE spectrum of gaseous indole showed two distinct features, one centered at 289.89 eV arising from the six carbon atoms not bound to nitrogen and one centered at 290.86 eV arising from the two carbon atoms directly bound to nitrogen [34], based on gas-phase results. For aqueous-phase indole, these two features largely merge and we fitted the spectrum simultaneously with two groups of Gaussian functions (6 + 2). Thus, the characteristic fitted parameters were mainly the two independent peak positions. The FWHM for each Gaussian function was fit to be 1.12 eV, which is fully consistent with values

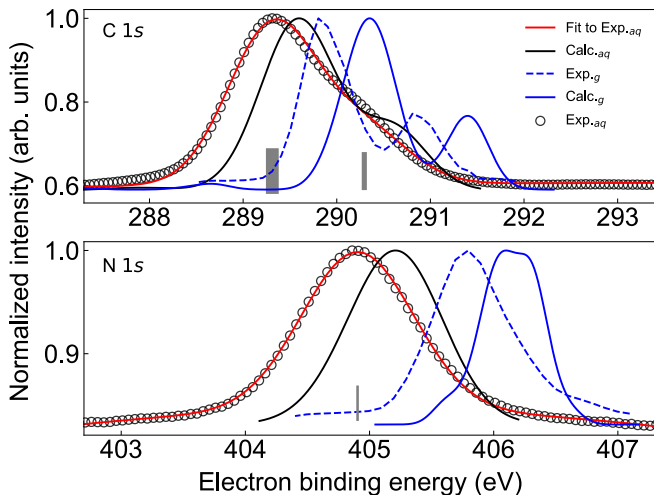


FIG. 4.  $C(1s)$  (upper panel) and  $N(1s)$  (lower panel) photoelectron spectra of indole. Gray empty circles represent the experimental data and red solid lines represent the overall fit for aqueous indole. The light-gray bars indicate the central positions for the individual Gaussians used to fit. The black and blue solid lines represent the simulated spectra for aqueous indole and gas-phase indole, respectively. The blue dashed lines are experimental data reported for indole in the gas phase [34].

TABLE II.  $C(1s)$  and  $N(1s)$  experimental and calculated binding energies (eV) for aqueous and gas-phase indole.

Peak	Exp. <sub>aq</sub>	Calc. <sub>aq</sub>	Exp. <sub>g</sub> <sup>a</sup>	Calc. <sub>g</sub>
$C^{1-6}$	289.31	289.59	289.89	290.34
$C^{7-8}$	290.29	290.58	290.86	291.39
$N^1$	404.90	405.28	405.82	406.15

<sup>a</sup> Gas-phase ionization energies reported in [34].

typically found for photoionization of neutral molecules of a similar size in solution. For the  $N(1s)$  PE spectrum, resulting from the single nitrogen atom in indole, one Gaussian centered at 404.90 eV with a FWHM of 1.06 eV was used to fit the spectrum. Compared to the reported gas-phase data [34], we obtained solvent-induced shifts of  $\sim 0.57$  eV for  $C(1s)$  and  $\sim 0.92$  eV for  $N(1s)$ .

The  $N(1s)$  and  $C(1s)$  BEs for aqueous-phase and gaseous indole from both the experiment and our calculations are shown in Tab. II. Note that the calculated values for  $C(1s)$  were obtained by fitting the simulated  $C(1s)$  core-level PE spectrum with the same fitting procedure as for the experimental spectrum. The FWHM of each Gaussian in the fit for the  $C(1s)$  simulated spectrum is 0.92 eV. The simulated  $N(1s)$  spectrum for aqueous indole is centered at 405.28 eV with a FWHM of 0.58 eV. The calculated PE spectra for the  $N(1s)$  and  $C(1s)$  electrons from gas-phase and aqueous-phase indole were shifted with respect to the experiment by  $\sim 0.3$ – $0.4$  eV, which is quite acceptable for these large absolute energies. More importantly, the calculations well reproduce the shapes of the spectra in both the gas and liquid phase, including the broadening upon solvation and the solvent shift; see Fig. 4. Even the  $C(1s)$  spectrum corresponding to convoluted signals from eight different carbon-atom sites in the molecule is described well for both aqueous and gas-phase indole.

### Solvation structure

While valence electrons are to a large extent delocalized, core electrons are localized near one of the nuclei. X-ray PES is thus suited for investigating the local or nearest-neighbor hydrogen-bonding structures by analyzing core-level chemical and solvent shifts as well as peak profiles arising from the intermolecular interaction of indole with surrounding water molecules [88].

The solvent-induced shift for the valence,  $C(1s)$ , and  $N(1s)$  signals are significantly different. This is indicative of the specific solvation structure near the ionized molecules. Energy shifts are approximately 0.47 eV for the valence ionization, 0.57 eV for the  $C(1s)$  ionization, and 0.92 eV for the  $N(1s)$  ionization.

When we examine the geometries of the microhydrated indole, Fig. 3, it is clear that one closest water molecule

tends to approach the nitrogen atom to form a direct N-H $\cdots$ O hydrogen bond, reflecting the structure of the gas-phase indole-water dimer [10]. This leads to a larger solvent stabilization of the core-ionized nitrogen atom as the water molecule’s dipole is pointing at indole’s N, i.e., the water is oriented toward N-H with its oxygen atom. On the other hand, core-ionized carbons are destabilized by the arrangement of the other water molecules. Those waters are hydrogen-oriented toward the indole ring. Therefore, the positively charged core holes on carbon atoms created by the ionization interact with partial positive charges of water’s hydrogen atoms.

This interpretation is further supported by calculations showing how calculated core- and valence-ionization energies of indole change upon adding explicit solvent molecules and introducing the polarizable continuum representing bulk water, see Tab. III. We observed that the addition of a single water molecule coordinated to the nitrogen atom causes a large decrease in the N(1s) binding energy, and this holds even when placing the system into a dielectric environment. The effect of this hydrogen-bound water molecule on the valence- and C(1s)-electron energies is much smaller. This is related to the delocalized character of the valence-electron hole and to the diffuse hydrogen-bond arrangements around the core-ionized carbon atoms, respectively.

### Auger electrons

Measured Auger-electron spectra following N(1s) and C(1s) ionization of aqueous indole, after fitted background subtraction, are shown in Fig. 5. Spectra were then fitted with five Gaussians in the case of C-Auger, and three Gaussians for N-Auger spectra, see Fig. 5. The two sharp peaks at a kinetic energy (KE) of  $\sim 396$  eV next to the N-Auger spectrum arose from the core ionization of Cl(2p) orbitals. These features occur due to the small amount of NaCl we added to the solution, *vide supra*.

The high-kinetic-energy onsets of N(1s) and C(1s) Auger spectra are 387.53 eV and 274.31 eV, respectively, and the FWHM of both Auger spectra are  $\sim 25$  eV, which are estimated based on the multiple Gaussian fitting for the spectra after the fitted background subtraction. The onset of the Auger spectra is defined in this work as the sum of the peak position and its FWHM of the most pronounced Gaussian function used to fit the spectrum, which is centered at 372.33 eV with a FWHM of 15.20 eV in the case of N-Auger, and at 259.58 eV with a FWHM of 14.73 eV in the case of C-Auger. As can be seen in Fig. 5, the C- and N-Auger spectra of aqueous indole have broad structures. Similar to that for gaseous indole [34], the broadening includes the finite line width of the x-ray PES, the vibrational distributions of the core-hole states and the final states, the core-hole lifetime, the analyzer resolution, and the contributions from the solvation

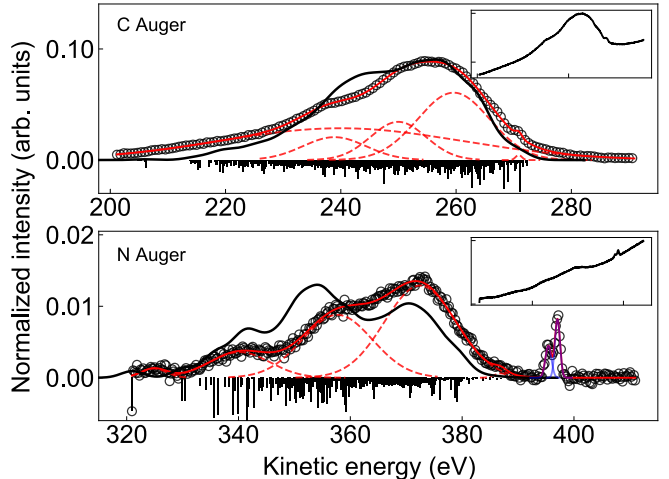


FIG. 5. C-Auger and N-Auger spectra (black circles) of aqueous-phase indole after fitted background subtraction. Red solid lines represent the overall fit and the red dashed lines are the individual fitted Gaussian. The black solid lines represent the simulated carbon/nitrogen 1s Auger spectrum in both panels. Contributions from the ionization of Cl(2p) are included in the fit and shown as blue solid lines. The downward-facing sticks schematically represent the population of involved two-hole states. The insets show the raw experimental Auger spectra. A global fit using second-order polynomials for the contributions of the scattered-electron background, with highly asymmetric spectral structure, was applied.

for aqueous indole. The multiple Gaussian contributions reflect Auger transitions involving several lower-lying energy states. This is detailed by *ab initio* modeling of the spectra. The black solid lines in Fig. 5 show the calculated Auger spectrum, following the ionization of both the carbon and nitrogen 1s electrons. The experimental spectrum is reasonably well reproduced for both cases, exhibiting also the experimentally observed substructure. Note, however, that the Auger peaks are formed by groups of large number of final states, the peaks can thus not be interpreted as a result of a single decay channel.

The calculated onsets of the Auger spectra of aqueous indole are also shown in Tab. IV. The electron holes of the final state correspond to the ejected  $\pi$  electrons of the indole ring, see HOMO and HOMO-1 orbitals in Fig. 2. Calculated values for gas-phase indole are 384.74 eV and 269.79 eV for N- and C-Auger electrons respectively, in a good agreement with recently published experimental data [34]. The calculated solvent shift for nitrogen and carbon Auger energies is 2.28 and 2.47 eV, respectively. Comparing the shifts, we again confirm the higher N(1s) core-ionized solvent stabilization relative to the C(1s) core-ionized state.

TABLE III. Calculated ionization energies (eV) of gas-phase and aqueous indole containing 0 – 3 explicit water molecules. “Solvated cluster” refers to a system placed into a dielectric environment to mimic non-specific solvation effects. For clarity, C(1s) ionization energies are averaged for six (1–6) and two (7–8) carbon atoms, which exhibit very similar energies.

$n_{water}$	Gas-phase cluster					Solvated cluster				
	HOMO	HOMO-1	N(1s)	C <sup>1-6</sup> (1s)	C <sup>7-8</sup> (1s)	HOMO	HOMO-1	N(1s)	C <sup>1-6</sup> (1s)	C <sup>7-8</sup> (1s)
0	7.87	8.29	406.24	290.15	291.24	7.13	7.57	405.28	289.39	290.43
1	7.51	7.94	405.55	289.82	290.82	7.03	7.48	404.95	289.32	290.30
2	8.02	8.42	405.99	289.72	291.28	7.22	7.64	405.15	289.46	290.45
3	7.93	8.33	405.74	290.21	291.17	7.18	7.60	404.98	289.43	290.40

TABLE IV. Summary of the measured and calculated BEs (eV) for valence, N(1s), and C(1s) ionization, and the KE onsets of the Auger electrons, for aqueous indole.

	Exp. fitting		Simulations	
	BE	KE onset	BE	KE onset
HOMO	7.38	–	7.22	–
HOMO-1	7.93	–	7.77	–
N(1s)	404.90	–	405.28	–
C <sup>1-6</sup> (1s)	289.31	–	289.59	–
C <sup>7-8</sup> (1s)	290.29	–	290.58	–
N Auger	–	387.53	–	387.02
C Auger	–	274.31	–	272.26

## CONCLUSIONS

We provided the first full photoemission spectrum of indole in aqueous solution by measuring the valence and core-level photoelectron and Auger spectra following ionization by 600 eV synchrotron radiation. Experimental spectra are interpreted with the help of high-level *ab initio* calculations. All characteristic peaks of aqueous-phase indole were assigned and the explicit and global solvent-induced energy shifts were extracted and supported by the calculations.

The lowest-binding-energy valence photoelectron peaks correspond to the ionization of the HOMO and HOMO-1 electrons, with binding energies of 7.38 and 7.93 eV, respectively. The observed solvent-induced shifts were relatively small in comparison with other neutral molecules of a similar size. This is due to delocalized valence electrons and competing specific and non-specific solvation effects. From the valence spectra, we also determined the reorganization energy, connecting photoelectron spectroscopy with electrochemical descriptors such as the redox potential.

Indole, in the gas phase, is known to form strong hydrogen-bonded complexes with water with its N-H group serving as the hydrogen-bond donor [10]. Our results demonstrate that this motif is also dominant in aqueous solution. Specifically, disentangling the solvent-induced shifts, which are specific extensions of the general chemical shift, in the core-ionization spectra enabled us to elucidate the solvent structure around the indole molecule. The core-level binding energies for nitrogen and carbon

1s electrons clearly indicated the presence of specific solvent effects due to a strong hydrogen bonding to nitrogen together with further non-specific effects due to solvent polarization. On the one hand, there is a strong directed and specific hydrogen bonding N-H $\cdots$ OH<sub>2</sub>, while on the other hand, there are unstructured interactions of the water solvent with the overall molecular structure.

Furthermore, we reported and interpreted the Auger spectra, which exhibit larger solvent shifts than the direct photoelectrons. These Auger-electron signals are brought about by many final dicationic states. A computational technique based on electron-population analysis was demonstrated as an efficient tool for modeling Auger spectra, aiding in further analysis of molecules in complex environments using x-ray photoemission spectroscopy.

Overall, our detailed investigation of the photoemission spectrum of indole in water provided a clear and refined view on the solvation of indole, specifically for its different moieties, including a surprising highly specific single-solvent molecule binding motif combined with further unspecific solvent interactions. From the perspective of computational chemistry, our work demonstrated the wide applicability of the maximum-overlap method, enabling us to model the ionic states through standard ground-state quantum chemical methods, combined with the non-equilibrium dielectric modeling of the environment.

## AUTHOR CONTRIBUTIONS

J.K., B.W., and P.S. conceived and supervised the project. L.H., S.M., F.T., S.T., J.K., and B.W. performed the x-ray-spectroscopy experiment. L.T., M.B., and P.S. carried out the simulations. All authors discussed the results and prepared the manuscript.

## DATA AND CODE AVAILABILITY

The data of relevance to this study have been deposited on Zenodo at DOI: 10.5281/zenodo.6519525.

Code availability: The ABIN code for molecular dynamics v. 1.1-alpha was used, available at <https://>

github.com/PHOTOX/ABIN. The Packmol code v. 18.169 was used, available at <http://leandro.iqm.unicamp.br/m3g/packmol/download.shtml>. Terachem v. 1.93 was used, available at <https://store.petachem.com>. Q-Chem v. 4.3 was used, available at <https://www.q-chem.com>.

## CONFLICTS OF INTEREST

There are no conflicts to declare.

## ACKNOWLEDGMENTS

We acknowledge Dr. Claudia Kolbeck for the help during the experimental campaign. We thank the PETRA III P04 beamline staff and Moritz Hoesch in particular as well as the DESY photon science chemistry-laboratory and crane operators for their assistance.

We acknowledge support by Deutsches Elektronen-Synchrotron DESY, a member of the Helmholtz Association (HGF), and the use of the Maxwell computational resources operated at Deutsches Elektronen-Synchrotron DESY. Parts of this research were carried out at PETRA III at DESY; beamtime was allocated for proposal II-20180012. This work was supported by the Cluster of Excellence "Advanced Imaging of Matter" (AIM, EXC 2056, ID 390715994) of the Deutsche Forschungsgemeinschaft (DFG) and by the European Research Council under the European Union's Seventh Framework Program (FP7/2007-2013) through the Consolidator Grant COMOTION (614507). L.H. acknowledges support by the National Natural Science Foundation of China (11704147) and a fellowship within the framework of the Helmholtz-OCPC postdoctoral exchange program. P.S., L.T., and M.B. thank the Czech Science Foundation (EXPRO project no. 21-26601X). B.W. acknowledges funding from the European Research Council (ERC) under the European Union's Horizon 2020 research and investigation programme (grant agreement 883759). F.T. and B.W. acknowledge support by the MaxWater initiative of the Max-Planck-Gesellschaft.

## REFERENCES

- || Petr.Slavicek@vscht.cz  
 § winter@fhi-berlin.mpg.de  
 \* jochen.kuepper@cifel.de;  
<https://www.controlled-molecule-imaging.org>
- [1] A. L. Sobolewski, W. Domcke, C. Dedonder-Lardeux, and C. Jouvet, Excited-state hydrogen detachment and hydrogen transfer driven by repulsive  $^1\pi\sigma^*$  states: A new paradigm for nonradiative decay in aromatic biomolecules, *Physical Chemistry Chemical Physics* **4**, 1093 (2002).
  - [2] O. Plekan, V. Feyer, R. Richter, M. Coreno, and K. C. Prince, Valence photoionization and photofragmentation of aromatic amino acids, *Molecular Physics* **106**, 1143 (2008).
  - [3] A. Chrostowska, S. Xu, A. Mazière, K. Boknevtz, B. Li, E. R. Abbey, A. Dargelos, A. Graciaa, and S.-Y. Liu, UV-photoelectron spectroscopy of BN indoles: experimental and computational electronic structure analysis., *Journal of the American Chemical Society* **136**, 11813 (2014).
  - [4] J. T. Vivian and P. R. Callis, Mechanisms of tryptophan fluorescence shifts in proteins, *Biophysical Journal* **80**, 2093 (2001).
  - [5] K. S. Sarkisyan, I. V. Yampolsky, K. M. Solntsev, S. A. Lukyanov, K. A. Lukyanov, and A. S. Mishin, Tryptophan-based chromophore in fluorescent proteins can be anionic, *Scientific Reports* **2**, 608 (2012).
  - [6] K. W. Short and P. R. Callis, Evidence of pure  $^1L_b$  fluorescence from redshifted indole-polar solvent complexes in a supersonic jet, *Journal of Chemical Physics* **108**, 10189 (1998).
  - [7] P. R. Callis, Molecular orbital theory of the  $^1L_b$  and  $^1L_a$  states of indole, *The Journal of Chemical Physics* **95**, 4230 (1991).
  - [8] C. Brand, J. Küpper, D. W. Pratt, W. L. Meerts, D. Krügler, J. Tatchen, and M. Schmitt, Vibronic coupling in indole: I. theoretical description of the  $^1L_a$ - $^1L_b$  interaction and the electronic spectrum, *Physical Chemistry Chemical Physics* **12**, 4968 (2010).
  - [9] J. Küpper, D. W. Pratt, W. L. Meerts, C. Brand, J. Tatchen, and M. Schmitt, Vibronic coupling in indole: II. investigation of the  $^1L_a$ - $^1L_b$  interaction using rotationally resolved electronic spectroscopy, *Physical Chemistry Chemical Physics* **12**, 4980 (2010).
  - [10] T. M. Korter, D. W. Pratt, and J. Küpper, Indole-H<sub>2</sub>O in the gas phase. Structures, barriers to internal motion, and S<sub>1</sub> ← S<sub>0</sub> transition moment orientation. Solvent reorganization in the electronically excited state, *The Journal of Physical Chemistry A* **102**, 7211 (1998).
  - [11] T. S. Zwier, Laser spectroscopy of jet-cooled biomolecules and their water-containing clusters: Water bridges and molecular conformation, *The Journal of Physical Chemistry A* **105**, 8827 (2001).
  - [12] H. Lippert, V. Stert, L. Hesse, C. P. Schulz, I. V. Hertel, and W. Radloff, Ultrafast photoinduced processes in indole-water clusters, *Chemical Physics Letters* **376**, 40 (2003).
  - [13] J. Onvlee, S. Trippel, and J. Küpper, Ultrafast light-induced dynamics in solvated biomolecules: The indole chromophore with water (2021), under review, arXiv:2103.07171 [physics].
  - [14] P. Meredith, B. J. Powell, J. Riesz, S. P. Nighswander-Rempel, M. R. Pederson, and E. G. Moore, Towards

- structure–property–function relationships for eumelanin, *Soft Matter* **2**, 37 (2006).
- [15] P. Meredith and T. Sarna, The physical and chemical properties of eumelanin, *Pigment Cell Research* **19**, 572 (2006).
- [16] G. Berden, W. L. Meerts, and E. Jalviste, Rotationally resolved ultraviolet spectroscopy of indole, indazole, and benzimidazole: Inertial axis reorientation in the  $S_1(^1L_b) \leftarrow S_0$  transitions, *The Journal of Chemical Physics* **103**, 9596 (1995).
- [17] T. J. Godfrey, H. Yu, M. S. Biddle, and S. Ullrich, A wavelength dependent investigation of the indole photo-physics *via* ionization and fragmentation pump–probe spectroscopies, *Physical Chemistry Chemical Physics* **17**, 25197 (2015).
- [18] R. Livingstone, O. Schalk, A. E. Boguslavskiy, G. Wu, L. T. Bergendahl, A. Stolow, M. J. Paterson, and D. Townsend, Following the excited state relaxation dynamics of indole and 5-hydroxyindole using time-resolved photoelectron spectroscopy, *The Journal of Chemical Physics* **135**, 194307 (2011).
- [19] M.-F. Lin, C.-M. Tseng, Y. T. Lee, and C.-K. Ni, Photodissociation dynamics of indole in a molecular beam, *The Journal of Chemical Physics* **123**, 124303 (2005).
- [20] A. L. Sobolewski and W. Domcke, Ab initio investigations on the photophysics of indole, *Chemical Physics Letters* **315**, 293 (1999).
- [21] T. Douki, The variety of UV-induced pyrimidine dimeric photoproducts in DNA as shown by chromatographic quantification methods, *Photochemical and Photobiological Sciences* **12**, 1286 (2013).
- [22] T. Ito, S. C. Baker, C. D. Stickley, J. G. Peak, and M. J. Peak, Dependence of the yield of strand breaks induced by  $\gamma$ -rays in DNA on the physical conditions of exposure: water content and temperature, *International Journal of Radiation Biology* **63**, 289 (1993).
- [23] E. Alizadeh, T. M. Orlando, and L. Sanche, Biomolecular damage induced by ionizing radiation: the direct and indirect effects of low-energy electrons on DNA, *Annual Review of Physical Chemistry* **66**, 379 (2015).
- [24] S. Lehnert, *Biomolecular Action of Ionizing Radiation* (CRC Press, London, 2007).
- [25] W. F. Morgan, Non-Targeted and Delayed Effects of Exposure to Ionizing Radiation: I. Radiation-Induced Genomic Instability and Bystander Effects In Vitro, *Radiation Research* **159**, 567 (2003).
- [26] J. R. Milligan, J. A. Aguilera, A. Ly, N. Q. Tran, O. Hoang, and J. F. Ward, Repair of oxidative DNA damage by amino acids, *Nucleic Acids Research* **31**, 6258 (2003).
- [27] C. Butchosa, S. Simon, and A. A. Voityuk, Electron transfer from aromatic amino acids to guanine and adenine radical cations in  $\pi$  stacked and T-shaped complexes, *Organic and Biomolecular Chemistry* **8**, 1870 (2010).
- [28] G. Merenyi, J. Lind, and X. Shen, Electron transfer from indoles, phenol, and sulfite ( $\text{SO}_3^{2-}$ ) to chlorine dioxide ( $\text{ClO}_2$ ), *The Journal of Physical Chemistry* **92**, 134 (1988).
- [29] A. Bernas, D. Grand, and E. Amouyal, Photoionization of solutes and conduction band edge of solvents. indole in water and alcohols, *The Journal of Physical Chemistry* **84**, 1259 (1980).
- [30] J. H. D. Eland, Photoelectron spectra of conjugated hydrocarbons and heteromolecules, *International Journal of Mass Spectrometry and Ion Physics* **2**, 471 (1969).
- [31] L. J. Dolby, G. Hanson, and T. Koenig, The helium(He I) photoelectron spectra of N-methylisoindole and N-methylindole, *The Journal of Organic Chemistry* **41**, 3537 (1976).
- [32] L. N. Domelsmith, L. L. Munchausen, and K. N. Houk, Photoelectron spectra of psychotropic drugs. I. Phenethylamines, tryptamines, and LSD, *Journal of the American Chemical Society* **99**, 4311 (1977).
- [33] M. Kubota and T. Kobayashi, Electronic structures of melatonin and related compounds studied by photoelectron spectroscopy, *Journal of Electron Spectroscopy and Related Phenomena* **128**, 165 (2003).
- [34] O. Plekan, H. Sa'adeh, A. Ciavardini, C. Callegari, G. Cautero, C. Dri, M. Di Fraia, K. C. Prince, R. Richter, R. Sergo, L. Stebel, M. Devetta, D. Faccialà, C. Vozzi, L. Avaldi, P. Bolognesi, M. C. Castrovilli, D. Catone, M. Coreno, F. Zuccaro, E. Bernes, G. Fronzoni, D. Toffoli, and A. Ponzi, Experimental and theoretical photoemission study of indole and its derivatives in the gas phase, *The Journal of Physical Chemistry A* **124**, 4115 (2020).
- [35] G. Kumar, A. Roy, R. S. McMullen, S. Kutagulla, and S. E. Bradforth, The influence of aqueous solvent on the electronic structure and non-adiabatic dynamics of indole explored by liquid-jet photoelectron spectroscopy, *Faraday Discussions* **212**, 359 (2018).
- [36] R. Seidel, S. Thürmer, and B. Winter, Photoelectron Spectroscopy Meets Aqueous Solution: Studies from a Vacuum Liquid Microjet, *The Journal of Physical Chemistry Letters* **2**, 633 (2011).
- [37] P. R. Tentscher, R. Seidel, B. Winter, J. J. Guerard, and J. S. Arey, Exploring the Aqueous Vertical Ionization of Organic Molecules by Molecular Simulation and Liquid Microjet Photoelectron Spectroscopy, *The Journal of Physical Chemistry B* **119**, 238 (2015).
- [38] R. Seidel, K. Kraffert, A. Kabelitz, M. N. Pohl, R. Kraehnert, F. Emmerling, and B. Winter, Detection of the electronic structure of iron-(iii)-oxo oligomers forming in aqueous solutions, *Physical Chemistry Chemical Physics* **19**, 32226 (2017).
- [39] D. Ghosh, A. Roy, R. Seidel, B. Winter, S. Bradforth, and A. I. Krylov, First-principle protocol for calculating ionization energies and redox potentials of solvated molecules and ions: Theory and application to aqueous phenol and phenolate, *The Journal of Physical Chemistry B* **116**, 7269 (2012).
- [40] T. A. Pham, M. Govoni, R. Seidel, S. E. Bradforth, E. Schwegler, and G. Galli, Electronic structure of aqueous solutions: Bridging the gap between theory and experiments, *Science Advances* **3**, e1603210 (2017).
- [41] E. Pluhařová, P. Slavíček, and P. Jungwirth, Modeling Photoionization of Aqueous DNA and Its Components, *Accounts of Chemical Research* **48**, 1209 (2015).
- [42] A. T. B. Gilbert, N. A. Besley, and P. M. W. Gill, Self-Consistent Field Calculations of Excited States Using the Maximum Overlap Method (MOM), *The Journal of Physical Chemistry A* **112**, 13164 (2008).
- [43] J. Viehhaus, F. Scholz, S. Deinert, L. Glaser, M. Ilchen, J. Seltmann, P. Walter, and F. Siewert, The Variable Polarization XUV beamline P04 at PETRA III: Optics, mechanics and their performance, *Nuclear Instruments and Methods in Physics Research Section A: Accelerators, Spectrometers, Detectors and Associated Equipment* **710**, 151 (2013).
- [44] S. Malerz, H. Haak, F. Trinter, A. B. Stephansen, C. Kol-

- beck, M. Pohl, U. Hergenbahn, G. Meijer, and B. Winter, A setup for studies of photoelectron circular dichroism from chiral molecules in aqueous solution, *Review of Scientific Instruments* **93**, 015101 (2022).
- [45] B. Winter and M. Faubel, Photoemission from Liquid Aqueous Solutions, *Chemical Reviews* **106**, 1176 (2006).
- [46] M. Faubel, S. Schlemmer, and J. P. Toennies, A molecular beam study of the evaporation of water from a liquid jet, *Zeitschrift für Physik D Atoms, Molecules and Clusters* **10**, 269 (1988).
- [47] Y. Tang, H. Shen, K. Sekiguchi, N. Kurahashi, T. Mizuno, Y.-I. Suzuki, and T. Suzuki, Direct measurement of vertical binding energy of a hydrated electron, *Physical Chemistry Chemical Physics* **12**, 3653 (2010).
- [48] H. Shen, N. Kurahashi, T. Horio, K. Sekiguchi, and T. Suzuki, Direct Measurement of Vertical Electron Binding Energies of Solvated Electrons in Methanol and Ethanol, *Chemistry Letters* **39**, 668 (2010).
- [49] N. Preissler, F. Buchner, T. Schultz, and A. Lübcke, Electrokinetic charging and evidence for charge evaporation in liquid microjets of aqueous salt solution, *The Journal of Physical Chemistry B* **117**, 2422 (2013).
- [50] A. T. Shreve, M. H. Elkins, and D. M. Neumark, Photoelectron spectroscopy of solvated electrons in alcohol and acetonitrile microjets, *Chemical Science* **4**, 1633 (2013).
- [51] N. Kurahashi, S. Karashima, Y. Tang, T. Horio, B. Abulimiti, Y.-I. Suzuki, Y. Ogi, M. Oura, and T. Suzuki, Photoelectron spectroscopy of aqueous solutions: Streaming potentials of NaX (X = Cl, Br, and I) solutions and electron binding energies of liquid water and X<sup>-</sup>, *The Journal of Chemical Physics* **140**, 174506 (2014).
- [52] M. Ončák, L. Šišťák, and P. Slavíček, Can theory quantitatively model stratospheric photolysis? *Ab initio* estimate of absolute absorption cross sections of ClOOCl, *The Journal of Chemical Physics* **133**, 174303 (2010).
- [53] Š. Sršeň, J. Sita, P. Slavíček, V. Ladányi, and D. Heger, Limits of the Nuclear Ensemble Method for Electronic Spectra Simulations: Temperature Dependence of the (*E*)-Azobenzene Spectrum, *Journal of Chemical Theory and Computation* **16**, 6428 (2020).
- [54] Š. Sršeň and P. Slavíček, Optimal representation of the nuclear ensemble: Application to electronic spectroscopy, *Journal of Chemical Theory and Computation* **17**, 6395 (2021).
- [55] M. Ceriotti, G. Bussi, and M. Parrinello, Colored-Noise Thermostats à la Carte, *Journal of Chemical Theory and Computation* **6**, 1170 (2010).
- [56] P. Slavíček, M. Ončák, D. Hollas, and O. Svoboda, ABIN (2020).
- [57] I. S. Ufimtsev and T. J. Martinez, Quantum Chemistry on Graphical Processing Units. 3. Analytical Energy Gradients, Geometry Optimization, and First Principles Molecular Dynamics, *Journal of Chemical Theory and Computation* **5**, 2619 (2009).
- [58] A. V. Titov, I. S. Ufimtsev, N. Luehr, and T. J. Martinez, Generating efficient quantum chemistry codes for novel architectures, *Journal of Chemical Theory and Computation* **9**, 213 (2013).
- [59] Y. Shao, Z. Gan, E. Epifanovsky, A. T. Gilbert, M. Wormit, J. Kusmann, A. W. Lange, A. Behn, J. Deng, X. Feng, D. Ghosh, M. Goldey, P. R. Horn, L. D. Jacobson, I. Kaliman, R. Z. Khaliullin, T. Kuš, A. Landau, J. Liu, E. I. Proynov, Y. M. Rhee, R. M. Richard, M. A. Rohrdanz, R. P. Steele, E. J. Sundstrom, H. L. Woodcock III, P. M. Zimmerman, D. Zuev, B. Albrecht, E. Alguire, B. Austin, G. J. O. Beran, Y. A. Bernard, E. Berquist, K. Brandhorst, K. B. Bravaya, S. T. Brown, D. Casanova, C.-M. Chang, Y. Chen, S. H. Chien, K. D. Closser, D. L. Crittenden, M. Diedenhofen, R. A. DiStasio Jr., H. Do, A. D. Dutoi, R. G. Edgar, S. Fatehi, L. Fusti-Molnar, A. Ghysels, A. Golubeva-Zadorozhnaya, J. Gomes, M. W. Hanson-Heine, P. H. Harbach, A. W. Hauser, E. G. Hohenstein, Z. C. Holden, T.-C. Jagau, H. Ji, B. Kaduk, K. Khistyayev, J. Kim, J. Kim, R. A. King, P. Klunzinger, D. Kosenkov, T. Kowalczyk, C. M. Krauter, K. U. Lao, A. D. Laurent, K. V. Lawler, S. V. Levchenko, C. Y. Lin, F. Liu, E. Livshits, R. C. Lochan, A. Luenser, P. Manohar, S. F. Manzer, S.-P. Mao, N. Mardirossian, A. V. Marenich, S. A. Maurer, N. J. Mayhall, E. Neuscamman, C. M. Oana, R. Olivares-Amaya, D. P. O'Neill, J. A. Parkhill, T. M. Perrine, R. Peverati, A. Prociuk, D. R. Rehn, E. Rosta, N. J. Russ, S. M. Sharada, S. Sharma, D. W. Small, A. Sodt, T. Stein, D. Stück, Y.-C. Su, A. J. Thom, T. Tsuchimochi, V. Vanovschi, L. Vogt, O. Vydrov, T. Wang, M. A. Watson, J. Wenzel, A. White, C. F. Williams, J. Yang, S. Yeganeh, S. R. Yost, Z.-Q. You, I. Y. Zhang, X. Zhang, Y. Zhao, B. R. Brooks, G. K. Chan, D. M. Chipman, C. J. Cramer, W. A. Goddard III, M. S. Gordon, W. J. Hehre, A. Klamt, H. F. Schaefer III, M. W. Schmidt, C. D. Sherrill, D. G. Truhlar, A. Warshel, X. Xu, A. Aspuru-Guzik, R. Baer, A. T. Bell, N. A. Besley, J.-D. Chai, A. Dreuw, B. D. Dunietz, T. R. Furlani, S. R. Gwaltney, C.-P. Hsu, Y. Jung, J. Kong, D. S. Lambrecht, W. Liang, C. Ochsenfeld, V. A. Rassolov, L. V. Slipchenko, J. E. Subotnik, T. V. Voorhis, J. M. Herbert, A. I. Krylov, P. M. Gill, and M. Head-Gordon, Advances in molecular quantum chemistry contained in the Q-Chem 4 program package, *Molecular Physics* **113**, 184 (2015).
- [60] E. Cancès, B. Mennucci, and J. Tomasi, A new integral equation formalism for the polarizable continuum model: Theoretical background and applications to isotropic and anisotropic dielectrics, *The Journal of Chemical Physics* **107**, 3032 (1997).
- [61] A. K. Rappe, C. J. Casewit, K. S. Colwell, W. A. Goddard III, and W. M. Skiff, UFF, a full periodic table force field for molecular mechanics and molecular dynamics simulations, *Journal of the American Chemical Society* **114**, 10024 (1992).
- [62] M. Rubešová, V. Jurásková, and P. Slavíček, Efficient modeling of liquid phase photoemission spectra and reorganization energies: Difficult case of multiply charged anions, *Journal of Computational Chemistry* **38**, 427 (2017).
- [63] B. W. Silverman, *Density Estimation for Statistics and Data Analysis* (Chapman & Hall, London, 1986).
- [64] O. A. Vydrov and G. E. Scuseria, Assessment of a long-range corrected hybrid functional, *The Journal of Chemical Physics* **125**, 234109 (2006).
- [65] U. Salzner and R. Baer, Koopmans' springs to life, *The Journal of Chemical Physics* **131**, 231101 (2009).
- [66] E. Muchová and P. Slavíček, Beyond Koopmans' theorem: Electron binding energies in disordered materials, *Journal of Physics: Condensed Matter* **31**, 043001 (2018).
- [67] S. Grimme, Semiempirical GGA-type density functional constructed with a long-range dispersion correction, *Journal of Computational Chemistry* **27**, 1787 (2006).
- [68] E. Neria, S. Fischer, and M. Karplus, Simulation of activation free energies in molecular systems, *The Journal of*

- Chemical Physics **105**, 1902 (1996).
- [69] W. L. Jorgensen, J. Chandrasekhar, J. D. Madura, R. W. Impey, and M. L. Klein, Comparison of simple potential functions for simulating liquid water, *The Journal of Chemical Physics* **79**, 926 (1983).
- [70] L. Martínez, R. Andrade, E. G. Birgin, and J. M. Martínez, PACKMOL: A package for building initial configurations for molecular dynamics simulations, *Journal of Computational Chemistry* **30**, 2157 (2009).
- [71] M. Mitani, O. Takahashi, K. Saito, and S. Iwata, Theoretical molecular Auger spectra with electron population analysis, *Journal of Electron Spectroscopy and Related Phenomena* **128**, 103 (2003).
- [72] In the present study, no low-energy cut-off measurements from an electrically biased liquid jet have been performed. This is the reason why we cannot apply the more robust method for a determination of absolute electron binding energies, as recently reported in [44].
- [73] B. Winter, R. Weber, W. Widdra, M. Dittmar, M. Faubel, and I. V. Hertel, Full Valence Band Photoemission from Liquid Water Using EUV Synchrotron Radiation, *The Journal of Physical Chemistry A* **108**, 2625 (2004).
- [74] B. Winter, R. Weber, I. V. Hertel, M. Faubel, P. Jungwirth, E. C. Brown, and S. E. Bradforth, Electron Binding Energies of Aqueous Alkali and Halide Ions: EUV Photoelectron Spectroscopy of Liquid Solutions and Combined Ab Initio and Molecular Dynamics Calculations, *Journal of the American Chemical Society* **127**, 7203 (2005).
- [75] M. N. Pohl, E. Muchová, R. Seidel, H. Ali, Š. Sršeň, I. Wilkinson, B. Winter, and P. Slavíček, Do water's electrons care about electrolytes?, *Chemical Science* **10**, 848 (2019).
- [76] S. Gozem, R. Seidel, U. Hergenbahn, E. Lugovoy, B. Abel, B. Winter, A. I. Krylov, and S. E. Bradforth, Probing the Electronic Structure of Bulk Water at the Molecular Length Scale with Angle-Resolved Photoelectron Spectroscopy, *The Journal of Physical Chemistry Letters* **11**, 5162 (2020).
- [77] C. F. Perry, P. Zhang, F. B. Nunes, I. Jordan, A. von Conta, and H. J. Wörner, Ionization Energy of Liquid Water Revisited, *The Journal of Physical Chemistry Letters* **11**, 1789 (2020).
- [78] S. Thürmer, S. Malerz, F. Trinter, U. Hergenbahn, C. Lee, D. M. Neumark, G. Meijer, B. Winter, and I. Wilkinson, Accurate vertical ionization energy and work function determinations of liquid water and aqueous solutions, *Chemical Science* **12**, 10558 (2021).
- [79] E. Pluhařová, P. Jungwirth, S. E. Bradforth, and P. Slavíček, Ionization of Purine Tautomers in Nucleobases, Nucleosides, and Nucleotides: From the Gas Phase to the Aqueous Environment, *The Journal of Physical Chemistry B* **115**, 1294 (2011).
- [80] J. Hager, M. Ivanco, M. A. Smith, and S. C. Wallace, Solvation effects in jet-cooled van der Waals clusters: Two-color threshold photoionization spectroscopy of indole, indole-argon, indole-methane, indole-water and indole-methanol, *Chemical Physics Letters* **113**, 503 (1985).
- [81] S. Malerz, F. Trinter, U. Hergenbahn, A. Ghrist, H. Ali, C. Nicolas, C.-M. Saak, C. Richter, S. Hartweg, L. Nahon, C. Lee, C. Goy, D. M. Neumark, G. Meijer, I. Wilkinson, B. Winter, and S. Thürmer, Low-energy constraints on photoelectron spectra measured from liquid water and aqueous solutions, *Physical Chemistry Chemical Physics* **23**, 8246 (2021).
- [82] T. Vondrák, S.-i. Sato, and K. Kimura, Cation Vibrational Spectra of Indole and Indole-Argon van der Waals Complex. A Zero Kinetic Energy Photoelectron Study, *The Journal of Physical Chemistry A* **101**, 2384 (1997).
- [83] L. Rulíšek, On the Accuracy of Calculated Reduction Potentials of Selected Group 8 (Fe, Ru, and Os) Octahedral Complexes, *The Journal of Physical Chemistry C* **117**, 16871 (2013).
- [84] D. Bím, L. Rulíšek, and M. Srnc, Computational Electrochemistry as a Reliable Probe of Experimentally Elusive Mononuclear Nonheme Iron Species, *The Journal of Physical Chemistry C* **122**, 10773 (2018).
- [85] A. A. Isse and S. Gennaro, Absolute Potential of the Standard Hydrogen Electrode and the Problem of Interconversion of Potentials in Different Solvents, *The Journal of Physical Chemistry B* **114**, 7894 (2010).
- [86] P. Jennings, A. C. Jones, A. R. Mount, and A. D. Thomson, Electrooxidation of 5-substituted indoles, *Journal of the Chemical Society, Faraday Transactions* **93**, 3791 (1997).
- [87] J. M. Herbert, Structure of the aqueous electron, *Physical Chemistry Chemical Physics* **21**, 20538 (2019).
- [88] B. Winter, Liquid microjet for photoelectron spectroscopy, *Nuclear Instruments and Methods in Physics Research Section A: Accelerators, Spectrometers, Detectors and Associated Equipment* **601**, 139 (2009), special issue in honour of Prof. Kai Siegbahn.

## TABLE OF CONTENTS GRAPHICAL ABSTRACT

